Implementation of Radiation Boundary Conditions in the Finite Element Analysis of Electromagnetic Wave Propagation

Edmund Sumbar, *Member, IEEE*, Fred E. Vermeulen, *Member, IEEE*, and F. Steve Chute, *Member, IEEE*

Abstract—**"Radiation boundary conditions" are formulated which permit the simulation of two-dimensional electromagnetic wave phenomena with the finite element method using conventional elements over a bounded domain. Implementation of such boundary conditions preserves the symmetry of the global stiffness matrix with all the advantages that this implies, including economy of storage and solution. A number of wire-antenna systems have been modeled with this technique in a finite element computer program called FEAST. The results demonstrate good agreement with published reference data.**

I. Introduction

AMONG the many applications using electromagnetic radiation as a penetrating source of heat, the authors are investigating novel schemes for enhancing the recovery of highly viscous petroleum oil from underground deposits using subterranean electrodes and antennas [1]–[3]. To help understand the processes and to explore the technical and economic merits of electromagnetic heating of oil-bearing formations at radio frequencies, a numerical simulator called FEAST has been developed.

FEAST models the simultaneous propagation of electromagnetic fields and diffusion of heat through isotropic materials in which the electrical and thermal properties are generally inhomogeneous and temperature dependent. It provides an azimuthally symmetric two-dimensional solution for both the transient heat flow equation and Maxwell's equations, which, when coupled through the temperature-dependent material properties, govern the heating processes.

Because material inhomogeneities play a large role in the phenomena under consideration, the finite element method [4], with its straightforward approach to handling material properties, is the solution method adopted in FEAST. Other schemes, notably the method of moments [5] and the boundary element technique [6], treat the variation of material properties with difficulty. The finite element approach has the further desirable characteristic that the node density can be concentrated in those places where the solution varies most rapidly or where greatest accuracy is needed. This contrasts with typical finite difference grids.

The finite element method relies on the existence of a bounded spatial problem domain having a finite extent. Antenna radiation problems, however, such as the one being studied by the authors, are intrinsically unbounded, apparently making finite elements ill suited for such applications. Recognizing the versatility of the method, researchers in the field of wave propagation phenomena have nevertheless adapted the technique by either defining so-called infinite elements [7] or coupling an interior finite element solution to an exterior boundary element solution [8]. In this paper, we describe an alternative adaptation of the finite element method to unbounded problems in electromagnetic radiation. Rather than alter the basic method itself, we have devised a straightforward way to implement "radiation boundary conditions" at the outer elements of a conventional finite element mesh. By making use of such radiation boundary conditions in the electromagnetic solver within FEAST, we have been able to successfully predict the electrical characteristics of various antenna configurations.

The following sections outline our implementation of these radiation boundary conditions for a Galerkin formulation of the finite element method.

II. Finite Element Analysis of Maxwell's Equations

Preparatory to a discussion of the radiation boundary condition, let us examine the finite element discretization of Maxwell's equations that is implemented in FEAST. With such an analysis in hand, the computational benefits of the radiation-boundary-condition approach to modeling electromagnetic propagation will be more readily apparent.

FEAST is structured to provide a near-field solution to the problem of time-harmonic electromagnetic wave propagation from an antenna into an inhomogeneous medium. Possible geometries are restricted in FEAST to those exhibiting cylindrical symmetry in the azimuthal direction. In other words, the material properties σ, ϵ, and μ may vary spatially in the radial and axial directions but must be independent of the azimuthal coordinate ϕ. A typical geometry, in this case a generic dipole antenna, is depicted in Fig. 1.

Manuscript received March 6, 1990; revised September 4, 1990. This work was supported by the Alberta Oil Sands Technology and Research Authority and by the Natural Sciences and Engineering Research Council of Canada.

The authors are with the Department of Electrical Engineering, University of Alberta, Edmonton, Alberta, Canada T6G 2G7.

IEEE Log Number 9041073.

0018-9480/91/0200-0267$01.00 ©1991 IEEE

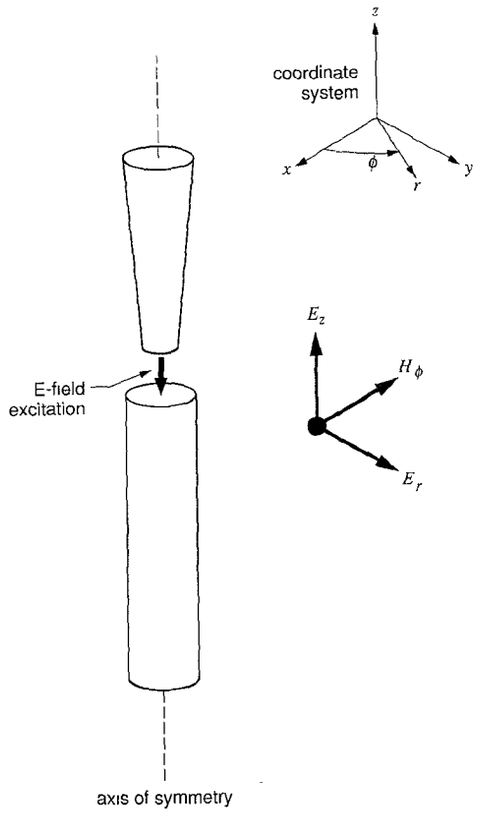

Fig. 1. The coordinate system imposed on a typical cylindrically symmetric wire antenna is shown along with the orientation of the electromagnetic field components.

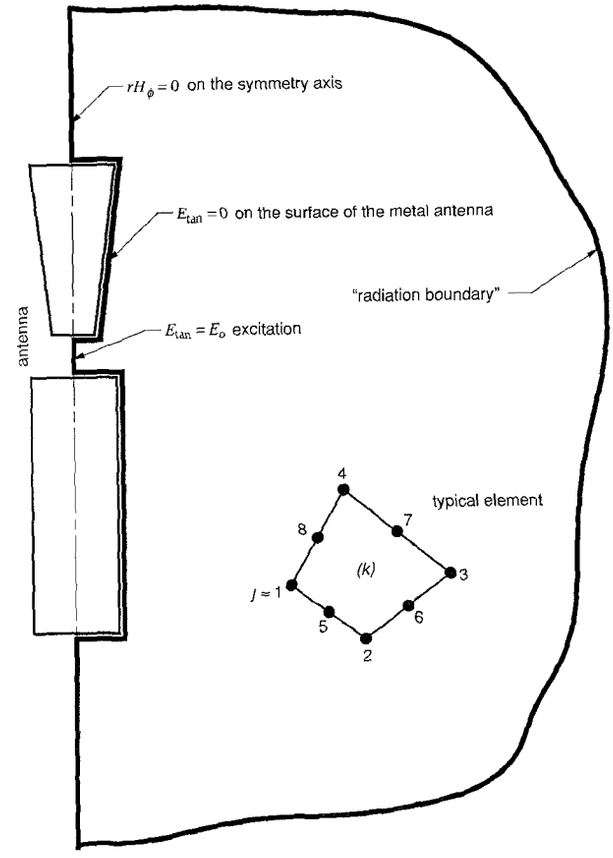

Fig. 2. A bounded problem domain that may be used to model the antenna described in Fig. 1. Either Dirichlet or Neumann boundary conditions must be specified at every point on the boundary. The interior of the domain is completely filled with a set of nonoverlapping elements such as the quadrilateral shown in the figure.

Assuming a time dependence of $e^{j\omega t}$, Maxwell's equations in time-harmonic form are written as

$$\nabla \times \boldsymbol{E} = -j\omega\mu \boldsymbol{H} \tag{1}$$

and

$$\nabla \times \boldsymbol{H} = (\sigma + j\omega\epsilon)\boldsymbol{E}. \tag{2}$$

Eliminating $\boldsymbol{E}$ from these two equations, we are left with the following:

$$\nabla \times \left[(\sigma + j\omega\epsilon)^{-1}\nabla \times \boldsymbol{H}\right] = -j\omega\mu \boldsymbol{H}. \tag{3}$$

Given the antenna in Fig. 1, which we assume to be excited by electric fields directed along the z axis, we can expect to find the $\boldsymbol{E}$ field confined to the $r-z$ plane and, perpendicular to this, a lone ϕ component of the $\boldsymbol{H}$ field. In general, both the $\boldsymbol{E}$ and $\boldsymbol{H}$ fields will be functions of r and z but will be independent of ϕ. Under these conditions, the vector equation (3) reduces to the scalar form

$$-\nabla_c \cdot \left[r^{-1}(\sigma + j\omega\epsilon)^{-1}\nabla_c(rH_\phi)\right] = -j\omega\mu H_\phi \tag{4}$$

where ∇_c is defined as a two-dimensional pseudo-Cartesian operator, namely,

$$\nabla_c \equiv \boldsymbol{a}_r \frac{\partial}{\partial r} + \boldsymbol{a}_z \frac{\partial}{\partial z}. \tag{5}$$

The operations indicated by (4) can be performed to give the following elliptical partial differential equation for the magnetic field component H_ϕ:

$$-\frac{\partial}{\partial r}\left(\frac{Y}{r}\frac{\partial rH_\phi}{\partial r}\right) - \frac{\partial}{\partial z}\left(\frac{Y}{r}\frac{\partial rH_\phi}{\partial z}\right) + \frac{Z}{r}rH_\phi = 0 \tag{6}$$

where

$$Y = (\sigma + j\omega\epsilon)^{-1} \quad \text{and} \quad Z = j\omega\mu. \tag{7}$$

The electric field components can be derived from (2) as

$$E_r = -\frac{Y}{r}\frac{\partial rH_\phi}{\partial z}$$

$$-E_z = -\frac{Y}{r}\frac{\partial rH_\phi}{\partial r}. \tag{8}$$

Equation (6) can be discretized and transformed into a weak or Galerkin form as described by Burnett [4]. To do this, we first define a problem domain by erecting a finite-sized boundary exterior to the antenna as depicted in Fig. 2. Part of this boundary lies on the symmetry axis, that is, the z axis, and the antenna surfaces. The remainder is the so-called radiation boundary, which is established at some distance away from the antenna. In general, the optimum location and shape for the radiation boundary is initially unknown and is established through a process of trial and error. Subsequently, a solution for $rH_\phi(r, z)$ is assumed to exist within individual finite elements that, patched together, con-

stitute the entire problem domain. For the kth such element, a trial solution for rH_ϕ can be assumed to take the following form [4], [9]:

$$rH_\phi^{(k)}(r,z) \approx \sum_{j=1}^{n} a_j N_j^{(k)}(r,z) = U^{(k)}(r,z). \tag{9}$$

Coefficients a_j are complex constants that remain to be determined, N_j are real-valued shape functions, and n represents the number of degrees of freedom or the number of nodes defining the kth element. Fig. 2 illustrates one of the many possible element types that may be used to fill in the domain: in this example, an eight-node quadrilateral is shown. Guidelines for the design of an appropriate mesh—the collection of elements that thoroughly patch the domain—can be found elsewhere [10], [11]. In FEAST, the shape functions N_j are two-dimensional isoparametric polynomials having the interpolatory property, namely, that $N_j = 1$ at node j and $N_j = 0$ at the other nodes making up the element. As a consequence of this, U at the node j will be equal to the coefficient a at that node:

$$U^{(k)}(r_j, z_j) = a_j. \tag{10}$$

The so-called Galerkin weighted residual equation is then formed for each element by substituting the trial solution, (9), into the governing equation (6), multiplying the result by the set of shape functions N_i, and integrating over the area of the element. For the kth element this procedure yields

$$\iint_{(k)} \left[-\frac{\partial}{\partial r}\left(\frac{Y}{r}\frac{\partial U^{(k)}}{\partial r}\right) - \frac{\partial}{\partial z}\left(\frac{Y}{r}\frac{\partial U^{(k)}}{\partial z}\right) + \frac{Z}{r}U^{(k)} \right] N_i^{(k)}\, dr\, dz = 0 \tag{11}$$

for $i = 1, 2, \cdots, n$. Equation (11) can be integrated by parts to give

$$\begin{aligned} &- \iint_{(k)} \left[\frac{\partial}{\partial r}\left(\frac{Y}{r}\frac{\partial U^{(k)}}{\partial r} N_i^{(k)}\right) + \frac{\partial}{\partial z}\left(\frac{Y}{r}\frac{\partial U^{(k)}}{\partial z} N_i^{(k)}\right) \right] dr\, dz \\ &\quad + \iint_{(k)} \left[\left(\frac{Y}{r}\frac{\partial U^{(k)}}{\partial r}\right)\frac{\partial N_i^{(k)}}{\partial r} \right. \\ &\quad \left. + \left(\frac{Y}{r}\frac{\partial U^{(k)}}{\partial z}\right)\frac{\partial N_i^{(k)}}{\partial z} + \frac{Z}{r}U^{(k)} N_i^{(k)} \right] dr\, dz = 0. \end{aligned} \tag{12}$$

Green's theorem in the $r-z$ pseudorectangular plane can then be applied to the first double integral in (12), transforming it into the following contour integral in which the path of integration follows the perimeter l of the element in a counterclockwise manner:

$$- \oint_{(k)} \left[\left(\frac{Y}{r}\frac{\partial U^{(k)}}{\partial r}\right)\cos\alpha^{(k)} + \left(\frac{Y}{r}\frac{\partial U^{(k)}}{\partial z}\right)\cos\beta^{(k)} \right] N_i^{(k)}\, dl. \tag{13}$$

The quantities $\cos\alpha^{(k)}$ and $\cos\beta^{(k)}$ are the direction cosines of the outward normal unit vector at a point along the perimeter. Equation (9) allows us to write (8) as

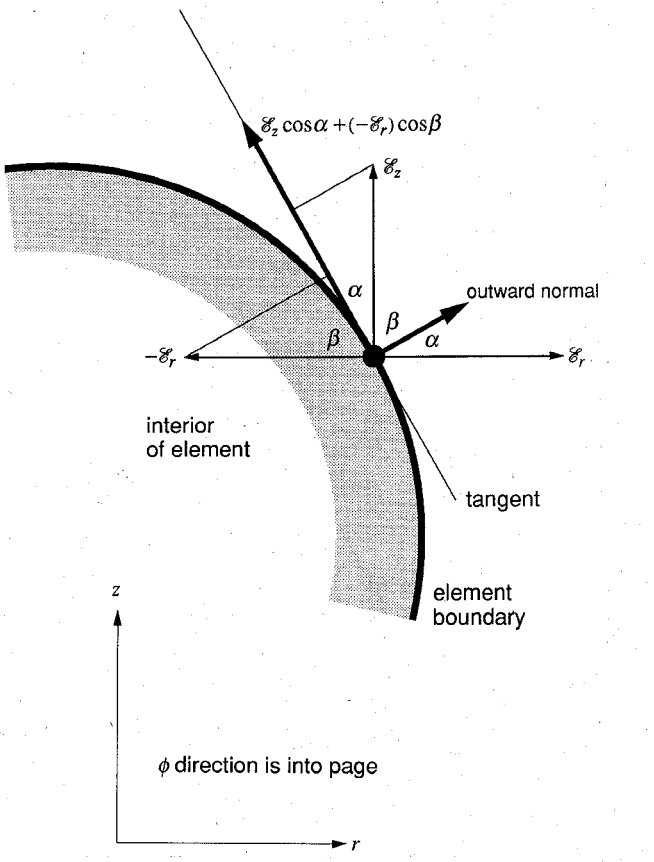

Fig. 3. Close-up of the surface of a typical finite element. The curvature of the element side is exaggerated to better show the vector relationships on the surface.

$$\begin{aligned} E_r^{(k)} &\approx -\frac{Y}{r}\frac{\partial U^{(k)}}{\partial z} = \mathscr{E}_r^{(k)} \\ -E_z^{(k)} &\approx -\frac{Y}{r}\frac{\partial U^{(k)}}{\partial r} = -\mathscr{E}_z^{(k)} \end{aligned} \tag{14}$$

and consequently, (13) as

$$- \oint_{(k)} \left[\left(\mathscr{E}_z^{(k)}\right)\cos\alpha^{(k)} + \left(-\mathscr{E}_r^{(k)}\right)\cos\beta^{(k)} \right] N_i^{(k)}\, dl. \tag{15}$$

The integrand of (15) has an important physical interpretation, which can be appreciated by studying Fig. 3. We see that the quantity in square brackets is the tangential electric field on a side of element k and is considered to have a positive sense when oriented in a counterclockwise direction. The concise form of (12) is therefore

$$\begin{aligned} &\iint_{(k)} \left[\left(\frac{Y}{r}\frac{\partial U^{(k)}}{\partial r}\right)\frac{\partial N_i^{(k)}}{\partial r} + \left(\frac{Y}{r}\frac{\partial U^{(k)}}{\partial z}\right)\frac{\partial N_i^{(k)}}{\partial z} + \frac{Z}{r}U^{(k)} N_i^{(k)} \right] dr\, dz \\ &\qquad = \oint_{(k)} \mathscr{E}_{\tan(\mathrm{CCW})}^{(k)} N_i^{(k)}\, dl, \qquad i = 1, 2, \cdots, n. \end{aligned} \tag{16}$$

Substituting the assumed trial solution, (9), into (16) results

in the following expression:

$$\sum_{j=1}^{n} a_j \iint_{(k)} \left[\frac{\partial N_i^{(k)}}{\partial r} \frac{Y}{r} \frac{\partial N_j^{(k)}}{\partial r} + \frac{\partial N_i^{(k)}}{\partial z} \frac{Y}{r} \frac{\partial N_j^{(k)}}{\partial z} + N_i^{(k)} \frac{Z}{r} N_j^{(k)} \right] dr\,dz$$

$$= \oint_{(k)} \mathscr{E}_{\tan(\mathrm{CCW})}^{(k)} N_i^{(k)}\, dl, \qquad i = 1,2,\cdots,n. \quad (17)$$

This expression constitutes the sought-after discretization of (6) for one element within the problem domain. Evaluation of (17) results in a system of n linear equations in n unknowns, the unknowns being the vector of a_j's. The undetermined coefficients a_j reflect the value of $U(\approx rH_\phi)$ at the n nodes of the element. The components of the matrix formed from the left-hand side of (17), the so-called stiffness terms, are symmetric about the diagonal. Ultimately, the element equations representing all the elements in the mesh are assembled into one large system. The coefficient matrix for this global system of equations, denoted by $[K]$, will be symmetric about its main diagonal and will be only sparsely populated by nonzero terms. The contour integrals on the right-hand side will be assembled into a vector $[f]$ which will incorporate nonzero electric field contributions from boundary nodes only—by definition, electric field boundary conditions are built into the Galerkin form of (6). After introducing additional boundary conditions, FEAST solves the system of linear equations

$$[K][a] = [f] \quad (18)$$

where $[a]$ is the solution vector representing the values of $U(\approx rH_\phi)$ at the nodes.

III. Applying Boundary Conditions

To ensure uniqueness, it is characteristic of field problems such as (6) that $U(\approx rH_\phi)$ be specified over part of the boundary defining the problem domain; that is, some Dirichlet boundary conditions must be enrolled in (18). As indicated in Fig. 2, the magnetic field on the symmetry axis of a cylindrical antenna must be zero, $U(r,z) = U_0 = 0$. On the conductive antenna surface, a Neumann condition is applied, namely, that the tangential electric field is zero, $\mathscr{E}_{\tan(\mathrm{CCW})}(r,z) = \mathscr{E}_0 = 0$. At the antenna feed, either a current or a voltage excitation may be implemented as nonzero Dirichlet or Neumann boundary conditions, respectively.

Over the radiation boundary illustrated in Fig. 2, neither U nor $\mathscr{E}_{\tan(\mathrm{CCW})}$ is known in advance. However, if the boundary is sufficiently far removed from the antenna and if the medium is homogeneous, we do know that

$$\boldsymbol{H} = \frac{\boldsymbol{n} \times \boldsymbol{E}}{\eta}. \quad (19)$$

The unit vector $\boldsymbol{n}$ points in the direction of propagation, which is radially outward from the center of the antenna, and η is the complex intrinsic impedance of the medium:

$$\eta = \sqrt{\frac{j\omega\mu}{\sigma + j\omega\epsilon}} = \sqrt{ZY}. \quad (20)$$

The integrand on the right-hand side of (17) can then be recast in terms of U by substituting

$$E_{\tan(\mathrm{CCW})} = -\eta H_\phi = -\frac{\eta}{r} rH_\phi \quad (21)$$

that is,

$$\mathscr{E}_{\tan(\mathrm{CCW})} \approx -\frac{\eta}{r} U = -\frac{\sqrt{ZY}}{r} U$$

$$\approx -\nu U. \quad (22)$$

Specification of $\mathscr{E}_{\tan(\mathrm{CCW})}$ in this way effectively implements an absorbing boundary condition. This approach will be strictly valid only in homogeneous media where the radiation boundary surface lies perpendicular to the direction of propagation and is located in the far field of the antenna. For cases not satisfying these conditions, a mathematically induced "reflected" wave will propagate from the radiation boundary into the problem domain, disrupting solution accuracy. In general, the degree to which these restrictions can be violated while still yielding accurate results is a matter of trial and error. It helps if the radiation boundary is approximately perpendicular to the direction of propagation and if the inhomogeneities are localized to the near-antenna region. Further, if the materials surrounding the antenna are electrically lossy, the magnitude of both the outgoing and "reflected" electromagnetic waves will be attenuated, and as a result, the accuracy of the near-antenna field solution will be less sensitive to the shape and location of the radiation boundary. The errors involved with the use of absorbing boundary conditions for problems in general wave motion have been discussed by Bayliss and Turkel [12] and Engquist and Majda [13].

Now, to apply (22) over an outside boundary of an external element, the trial solution (9) is substituted for U to give

$$\mathscr{E}_{\tan(\mathrm{CCW})}^{(k)}(r,z) \approx -\nu^{(k)} U^{(k)}(r,z) = -\nu^{(k)} \sum_{j=1}^{n} a_j N_j^{(k)}(r,z). \quad (23)$$

The force vector integral (right-hand side of (17)) is subsequently written as

$$\oint_{(k)} \mathscr{E}_{\tan(\mathrm{CCW})}^{(k)} N_i^{(k)}\, dl = -\oint_{(k)} \left(\nu^{(k)} \sum_{j=1}^{n} a_j N_j^{(k)} \right) N_i^{(k)}\, dl$$

$$= -\sum_{j=1}^{n} a_j \oint_{(k)} N_j^{(k)} \nu^{(k)} N_i^{(k)}\, dl,$$

$$i = 1,2,\cdots,n. \quad (24)$$

This quantity is algebraically similar to the stiffness terms, that is, those integrals on the left-hand side of (17). Essentially, the radiation boundary condition contributes additional terms in the coefficients a. As such, (18) may be expressed in closed form by transferring these additional terms from the right-hand to the left-hand side of (18). Fortunately, the interpolatory nature of the shape functions greatly simplifies the evaluation of the integral in (24). Moreover, the symmetry of the global stiffness matrix is preserved.

Ordinary Neumann boundary conditions are applied by evaluating the line integrals on the right-hand side of (17) with specified values of $\mathscr{E}_{\tan(\mathrm{CCW})}$. After all the Neumann conditions are set, the Dirichlet conditions are specified by constraining the solution vector to take on specified values at the nodes in question. Given the interpolatory nature of the shape functions, we arrange for $a_m = U_{0_m}$ at node m. This is

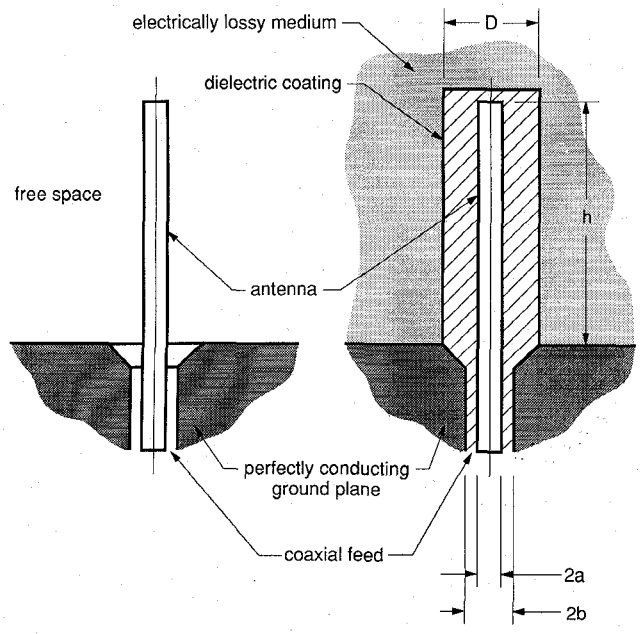

Fig. 4. Diagram of two monopole antenna configurations.

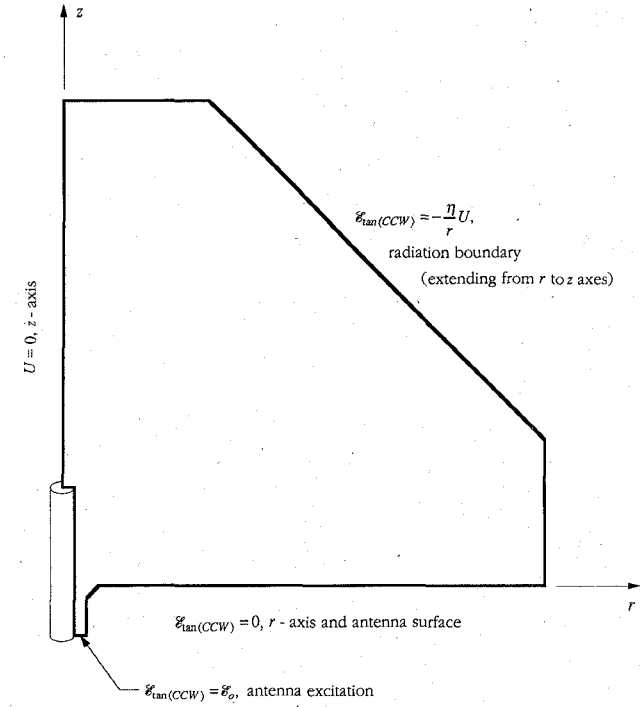

Fig. 5. The problem domain and boundary conditions used by FEAST to calculate the electromagnetic fields near the monopole antennas of Fig. 4.

accomplished in (18) with the following treatment:

$$\begin{bmatrix} K_{11} & \cdots & K_{1,m-1} & 0 & K_{1,m+1} \\ \vdots & & \vdots & \vdots & \vdots \\ K_{m-1,1} & \cdots & K_{m-1,m-1} & 0 & K_{m-1,m+1} \\ 0 & \cdots & 0 & 1 & 0 \\ K_{m+1,1} & \cdots & K_{m+1,m-1} & 0 & K_{m+1,m+1} \\ \vdots & & \vdots & \vdots & \vdots \\ K_{t1} & \cdots & K_{t,m-1} & 0 & K_{t,m+1} \end{bmatrix}$$

$$\begin{bmatrix} \cdots & K_{1t} \\ & \vdots \\ \cdots & K_{m-1,t} \\ \cdots & 0 \\ \cdots & K_{m+1,t} \\ & \vdots \\ \cdots & K_{tt} \end{bmatrix} \begin{bmatrix} a_1 \\ \vdots \\ a_m \\ \vdots \\ a_t \end{bmatrix} = \begin{bmatrix} f_1 - K_{1m}U_{0_m} \\ \vdots \\ f_{m-1} - K_{m-1,m}U_{0_m} \\ U_{0_m} \\ f_{m+1} - K_{m+1,m}U_{0_m} \\ \vdots \\ f_t - K_{tm}U_{0_m} \end{bmatrix}. \quad (25)$$

The subscript t refers to the total number of nodes associated with the mesh. A similar procedure is executed for every node at which a Dirichlet boundary condition is defined. Essentially, members of row m and column m in the stiffness matrix are replaced by zeros except on the diagonal, where a 1 is substituted. The force vector is then modified to take into account the presence of the boundary condition. Note that after (18) is solved, the solution at node m will be exactly the value specified.

The next section reviews some data generated by FEAST using the boundary conditions just described. All of the cases are problems in wire-antenna radiation.

IV. Typical Program Results

The analysis of two very different antenna configurations is presented here. In one case we have a bare monopole antenna radiating into free space, in the other a dielectric-coated monopole radiating into a lossy medium. Both antennas are situated above a perfectly conducting ground plane. The two configurations are illustrated in Fig. 4. Their electrical characteristics were calculated using the electrical-solver portion of FEAST. Utilizing the full capacity of the available computer hardware, a network of 424 quadratic isoparametric triangular and quadrilateral elements comprising 943 nodes was used to patch the finite element mesh. The problem domain was bounded as shown in Fig. 5.

Specifying as it does a homogeneous, lossless medium, the first case represents one of the simplest of antenna problems. FEAST was used to calculate the distribution of current along the surface of a bare monopole in free space at a frequency of 114 MHz. Antenna dimensions were as follows (refer to Fig. 4): $h/\lambda_0 = 0.375$, $a/\lambda_0 = 0.0254$, and $b/a = 1.189$, where λ_0 is the free-space wavelength. The result is compared in Fig. 6 with a theoretical model based on a transmission line analogy [14]. The current distribution was derived from the field quantity $U(\approx rH_\phi)$ along the surface of the antenna by evaluating the boundary condition for the tangential magnetic field at a perfect conductor, namely, $\boldsymbol{n} \times \boldsymbol{H} = \boldsymbol{J}_s$. Another parameter, driving point admittance, was obtained by dividing the current on the antenna at a point which is level with the ground plane by the interelectrode voltage at that location. A numerical integration of the r-directed electric field estimated this voltage. Fig. 7 compares the driving point admittances calculated with FEAST to a set of theoretical data for monopoles of varying length [14].

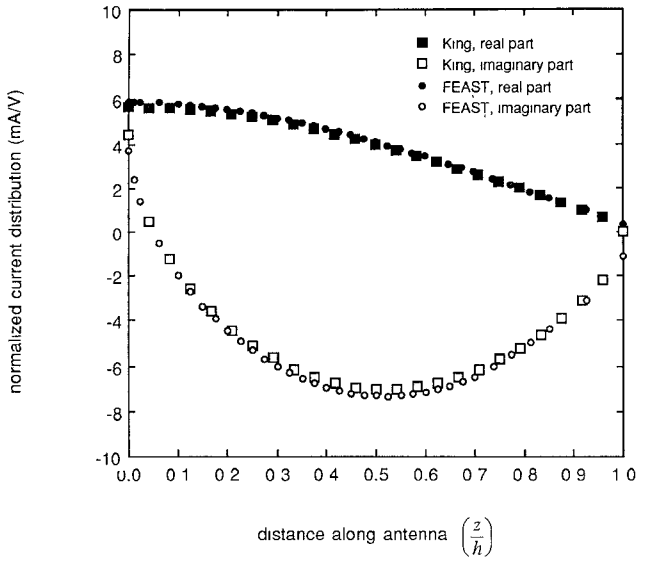

Fig. 6. Normalized antenna current distribution for a bare monopole over a perfectly conducting ground plane radiating into free space. The frequency is 114 MHz, $h/\lambda_0 = 0.375$, $a/\lambda_0 = 0.0254$, and $b/a = 1.189$ where λ_0 is the free-space wavelength. FEAST output is compared with theoretical data published by King [14].

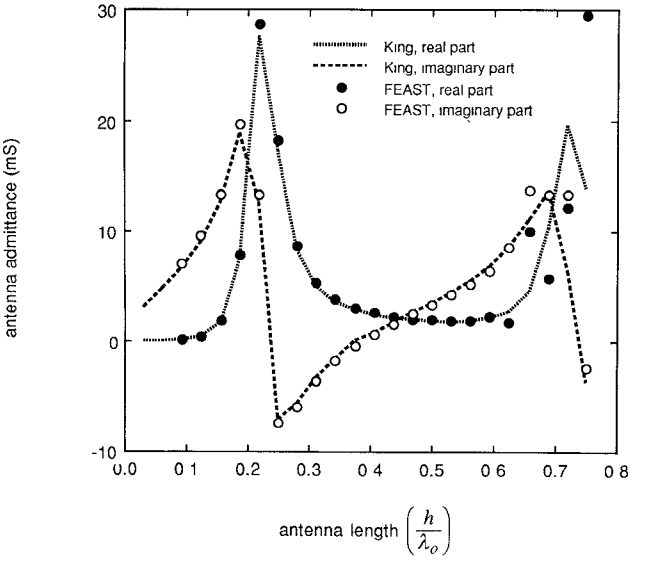

Fig. 7. Antenna driving point admittance versus antenna length for a bare monopole over a perfectly conducting ground plane radiating into free space. The frequency is 114 MHz, $a/\lambda_0 = 0.0064$, and $b/a = 1.189$, where λ_0 is the free-space wavelength. FEAST output is compared with theoretical data published by King [14].

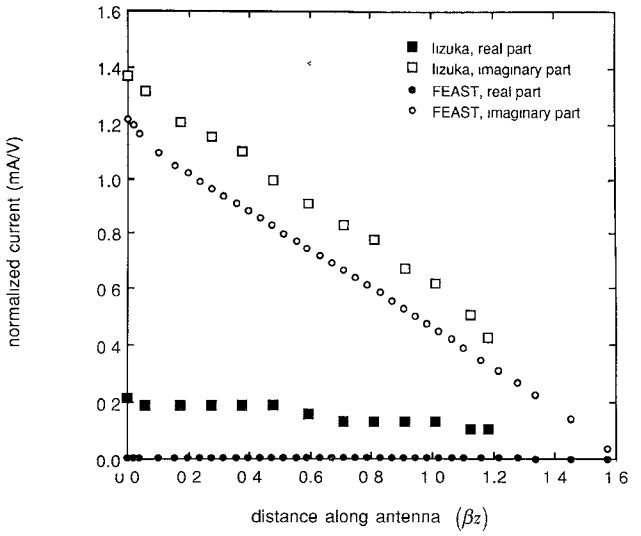

Fig. 8. Current distribution along a dielectric-coated monopole immersed in a lossy medium at a frequency of 114 MHz. Antenna dimensions and material properties are as follows: $\beta h = \pi/2$, where β is $2\pi/\lambda$ and λ is the wavelength in the lossy material, $2a = 0.25$ in. (6.35 mm), $b/a = 1.125$, $D/2a = 4$, ϵ_r (medium) = 78, ϵ_r (coating) = 1, and σ (medium) = 18×10^{-3} S/m. FEAST output is compared with experimental data published by Iizuka [15].

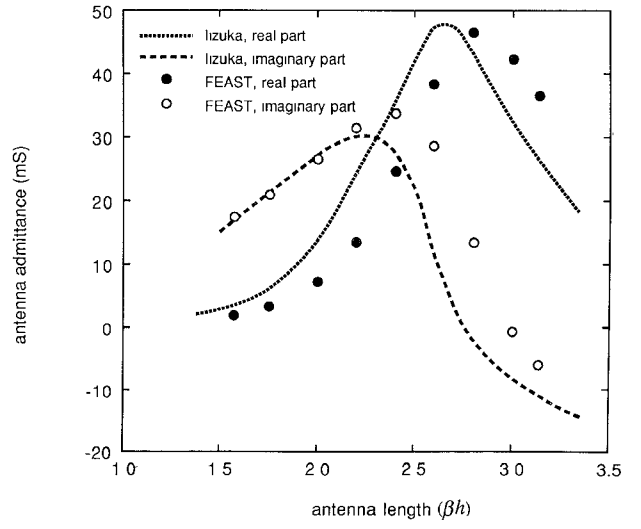

Fig. 9. Driving point admittances of dielectric-coated monopoles of varying length immersed in a lossy medium. The frequency is 114 MHz; β is $2\pi/\lambda$ and λ is the wavelength in the lossy material, $2a = 0.25$ in. (6.35 mm), $b/a = 1.125$, $D/2a = 1.25$, ϵ_r (medium) = 78, ϵ_r (coating) = 2.46, and σ (medium) = 18×10^{-3} S/m. FEAST output is compared with experimental data published by Iizuka [15].

The simulation results for the bare monopole in free space show very good agreement with selected theory. Some deviation is apparent in the admittance curve of Fig. 7 for long antenna lengths. This is probably a consequence of using too coarse a finite element mesh to model those cases, as the radial and axial extent of the mesh was scaled to be about 12 times h while the total number of nodes remained fixed.

A far more severe test of FEAST was to model insulated monopoles immersed in a lossy medium. A signal frequency of 114 MHz was applied to an antenna having a length $\beta h = \pi/2$, where β is $2\pi/\lambda$ and λ is the wavelength in the lossy material. The antenna diameter $2a$ was 0.25 in., and $b/a = 1.125$. The ratio of the diameter of the dielectric sheath, D, to the diameter of the antenna, $2a$, was 4.0; its dielectric constant was taken to be 1.0. For the lossy exterior medium, a dielectric constant of 78.0 and an electrical conductivity, σ, of 18×10^{-3} S/m were assumed. Again, the current distribution and driving point admittance were evalu-

ated. The results appear in Figs. 8 and 9. In this case, the program data are compared with the experimental results of Iizuka [15].

Results for the case of the coated monopole in a lossy medium are good; FEAST was able to satisfactorily replicate the general shape of the current distribution and admittance curves. In this instance, the accuracy of Iizuka's data may be suspect, as noted by others [16].

V. Conclusions

It is apparent from Figs. 6 through 9 that FEAST, with its novel radiation-boundary-condition approach to the simulation of electromagnetic propagation, can approximate the electrical characteristics of monopole antennas quite well. In addition to the antenna systems described here, other antenna configurations were tested, including bare dipoles in free space, bare dipoles in lossy materials, and insulated monopoles in free space. These simulations likewise yielded satisfactory results for the particular geometries considered [17].

The appeal of radiation boundary conditions for studying wave propagation in conjunction with the finite element method lies in their ease of implementation and in a reassuring physical interpretation. No special elements need to be designed; nor are additional analysis methods required, making it possible to introduce them into other existing computer codes.

References

[1] E. Sumbar, F. E. Vermeulen, and F. S. Chute, "Increasing oil production from a well with radio waves," in *Proc. 5th Annual Rev. Progress in Appl. Computat. Electromagn. Conf.* (Naval Postgraduate School, Monterey, CA), 1989, pp. 251–259.

[2] F. S. Chute and F. E. Vermeulen, "Present and potential applications of electromagnetic heating in the *in situ* recovery of oil," *AOSTRA J. Res.*, vol. 4, p. 19, 1988.

[3] F. E. Vermeulen and F. S. Chute, "Electromagnetic techniques in the *in situ* recovery of heavy oils," *J. Microwave Power*, vol. 18, no. 1, 1983.

[4] D. S. Burnett, *Finite Element Analysis: From Concepts to Applications*. Menlo Park, CA: Addison-Wesley, 1987.

[5] R. F. Harrington, *Field Computation by Moment Methods*. New York: Macmillan, 1968.

[6] C. A. Brebbia, *The Boundary Element Method for Engineers*. Plymouth: Pentech Press, 1984.

[7] M. J. McDougall and J. P. Webb, "Infinite elements for the analysis of open dielectric waveguides," *IEEE Trans. Microwave Theory Tech.*, vol. 37, p. 1724, 1989.

[8] K. D. Paulsen, D. R. Lynch, and J. W. Strohbehn, "Three-dimensional finite, boundary, and hybrid element solutions of the Maxwell equations for lossy dielectric media," *IEEE Trans. Microwave Theory Tech.*, vol. 36, p. 682, 1988.

[9] O. C. Zienkiewicz, *The Finite Element Method*. London: McGraw-Hill, 1977.

[10] J. F. Thompson, Z. U. A. Warsi, and C. W. Mastin, *Numerical Grid Generation: Foundations and Applications*. New York: Elsevier, 1985.

[11] J. Suhara and J. Fukuda, "Automatic mesh generation for finite element analysis," in *Advances in Computational Methods in Structural Mechanics and Design*, J. T. Oden, R. W. Clough, and Y. Yamamoto, Eds. Huntsville, AL: University of Alabama Press, 1972, pp. 607–624.

[12] A. Bayliss and E. Turkel, "Radiation boundary conditions for wave-like equations," *Commun. Pure Appl. Math.*, vol. 33, p. 707, 1980.

[13] B. Engquist and A. Majda, "Absorbing boundary conditions for the numerical solution of waves," *Math. Comput.*, vol. 31, p. 629, 1977.

[14] R. W. P. King, *Tables of Antenna Characteristics*. New York: IFI/Plenum, 1971.

[15] K. Iizuka, "An experimental study of the insulated dipole antenna immersed in a conducting medium," *IEEE Trans. Antennas Propagat.*, vol. AP-11, p. 518, 1963.

[16] A. H. J. Fleming and K. H. Joyner, "Moment method analysis of radiation and scattering by thin wires in an infinite dissipative medium," *Appl. Computat. Electromagn. Soc. J.* (Special Issue on Electromagnetic Computer Code Validation), Naval Postgraduate School, Monterey, CA, pp. 51–74, 1989.

[17] E. Sumbar, F. S. Chute, and F. E. Vermeulen, "A 2-D finite element model for wave propagation into arbitrary inhomogeneous materials," *Appl. Computat. Electromagn. Soc. J.*, vol. 4, no. 2, p. 27, 1989.

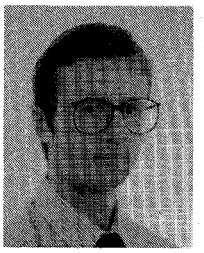

Edmund Sumbar (M'87) was born in Calgary, Canada, in 1954. He received the B.Sc. and Ph.D. degrees from the University of Alberta in electrical engineering.

After completing his studies, in 1984, his life-long interest in particle accelerators took him to the Stanford Linear Accelerator Center, where he worked in the high-power electronics division. Returning to the University of Alberta one year later as a research associate, he has since been developing electromagnetic modeling software on Macintosh computers.

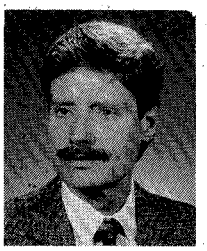

Fred E. Vermeulen (S'64–M'73) was born in Stuttgart, Germany. He received the B.Sc. degree from the University of Alberta, the M.A.Sc. degree from the University of British Columbia, and the Ph.D. degree from the University of Alberta in 1966, all in electrical engineering.

From 1966 to 1967 he was a National Research Council Postdoctoral Fellow at the European Organization for Nuclear Research at Geneva, Switzerland, where he was engaged in the study of space charge problems as related to the transport of ion beams. In 1967 he assumed an academic position at the University of Alberta, where he is currently Professor of Electrical Engineering. His research is in applied electromagnetics, a particular interest being the physical and numerical modeling of the electromagnetic heating of materials.

F. Steve Chute (S'60–M'65) received the M.A.Sc. degree from the University of British Columbia, Vancouver, B.C., Canada, in 1964 and the Ph.D. degree from the University of Alberta, Edmonton, Alta., Canada, in 1966, both in electrical engineering.

He served in the Canadian Armed Forces and was involved in the design and maintenance of radar and VHF/UHF communications systems. He began his academic career as an Assistant Professor at the Royal Military College in Kingston, Ont., Canada, and is presently a Professor in the Department of Electrical Engineering at the University of Alberta. His research work relates primarily to applied electromagnetics, with a special interest in the numerical and physical modeling of electromagnetic systems designed to heat materials.